Surface-Enhanced Raman Spectroscopy for Real-Time Monitoring of Reactive Oxygen Species-Induced DNA Damage and Its Prevention by Platinum Nanoparticles

Sajanlal R. Panikkanvalappil, Mahmoud A. Mahmoud,[#] Megan A. Mackey,[#] and Mostafa A. El-Sayed*

Laser Dynamics Laboratory, School of Chemistry and Biochemistry, Georgia Institute of Technology, Atlanta, Georgia 30332-0400, United States. [#]M.A. Mahmoud and M.A. Mackey contributed equally.

ABSTRACT We have successfully demonstrated the potential of surface-enhanced Raman spectroscopy (SERS) in monitoring the real time damage to genomic DNA. To reveal the capabilities of this technique, we exposed DNA to reactive oxygen species (ROS), an agent that has been implicated in causing DNA double-strand breaks, and the various stages of free radical-induced DNA damage have been monitored by using SERS. Besides this, we showed that prompt DNA aggregation followed by DNA double-strand scission and residual damage to the DNA bases caused by the ROS could be substantially reduced by the protective effect of Pt nanocages and nearly cubical Pt nanopartcles. The antioxidant activity of Pt nanoparticles was further confirmed by the cell viability studies. On the basis of SERS results, we identified various stages involved in the mechanism of action of ROS toward DNA damage, which involves the DNA double-strand scission and its aggregation followed by the oxidation of DNA bases. We found that Pt nanoparticles inhibit the DNA double-strand scission to a significant extent by the degradation of ROS. Our method illustrates the capability of SERS technique in giving vital information about the DNA degradation reactions at molecular level, which may provide insight into the effectiveness and mechanism of action of many drugs in cancer therapy.

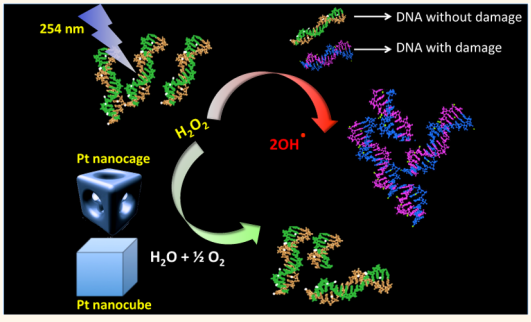

KEYWORDS: SERS · DNA damage · reactive oxygen species · Pt nanoparticles · real-time monitoring

Reactive oxygen species (ROS) are the byproducts of cellular metabolism, which may lead to DNA damage and eventually to cancer.[1] They are generally produced during cellular metabolism as well as from sources like drugs, radiation, and pollutants. Autoxidation of lipids leads to the formation of ROS such as H_2O_2,[2,3] which can easily diffuse through membranes and can induce DNA damage. Recent reports have demonstrated that certain nanoparticles can act as potent free radical scavengers and antioxidants.[4−6] These nanoparticle antioxidants are capable of reducing the concentration of reactive oxygen and nitrogen species. Being a stable inorganic catalyst for ROS scavenging, noble metal nanoparticles are unlikely to produce any secondary ROS compared to other conventional antioxidant molecules;[7] hence, they may become novel protective agents against ROS.

Identification of the structural modifications in genomic DNA is extremely important in medical diagnostics, as slight alterations in the DNA sequence may result in many diseases including cancer.[8] It is equally important to develop new free radical scavenging materials along with sensible methods to monitor various stages of DNA damages. In recent years, the sensitivity of detection of free radical-induced DNA damage has increased considerably.[9−11] A sensitive and reliable method capable of providing a better understanding of the detailed structural consequences at a molecular level during early events in DNA damage can give new insight into the early stage detection of many diseases. Though a variety of biological and

* Address correspondence to melsayed@gatech.edu.

Received for review March 8, 2013 and accepted August 17, 2013.

Published online August 17, 2013
10.1021/nn403722x

chemical methods exist to detect and characterize DNA damage, unfortunately many of these common biological techniques and chemical methods have limited sensitivity and are generally unable to monitor DNA damage in real time.[12,13]

As a noninvasive technique, Raman spectroscopy can be used to identify DNA marker bands that can be used to assign large-scale conformational states directly.[14−16] Surface enhanced Raman spectroscopy (SERS) is emerging as an important analytical tool for the ultrasensitive detection of various analytes.[17−21] More recently, the molecular fingerprinting capability of this method has been used for identifying mutations in DNA without the aid of any Raman labels.[22,23] The label-free DNA detection method gives direct information of DNA structure in comparison with methods utilizing SERS labels where the spectral features of the DNA itself are unimportant. Here, we report the capability of our SERS-based label-free DNA characterization technique for real-time monitoring of various molecular events during the ROS-induced damage within the genomic DNA. Further, the effectiveness of Pt nanoparticles in preventing the free radical-induced DNA damage was also probed using SERS.

RESULTS AND DISCUSSION

In our recent study, we had demonstrated the remarkable potential of SERS in revealing molecular fingerprints of genomic DNA using Ag NPs.[24] The method was capable of measuring reproducible SERS spectra of genomic DNA with high signal/noise ratio. Inspired from these results, in the current study, we investigated the chemical modifications involved during various stages of ROS-induced genomic DNA damage using SERS. Structural changes and chemical modifications in DNA during their interaction with ROS is important, as it helps to understand the mechanism of action and physiological role of ROS on DNA damage. In DNA, nucleobases and the deoxyribose sugar−phosphate backbone are susceptible for chemical modification by the interaction of hydroxyl radicals generated *via* UV (254 nm) photolysis of H_2O_2.[25,26] In this study, for monitoring the molecular events associated with ROS attack, a series of SERS spectra were collected in every 5 min from the DNA extracted from human karatinocyte (HaCaT) cells, while it was being exposed to H_2O_2/UV. The SERS spectra were collected by using a 5 nM solution of Ag NPs. High concentration of the nanoparticles virtually acts as *aggregated nanoparticles*, without touching each other, wherein a larger number of nanoparticles in the 3D volume would facilitate the excitation of a larger number of NPs by the laser, leading to significant enhancement of the Raman signals of DNA.[24]

We gave special attention to prevent the drying of DNA/Ag NPs solution throughout the SERS measurements, as DNA can undergo various conformational changes upon drying, which may interfere with the SERS results. Variations in the characteristic SERS bands revealing the DNA damage have been given in Figure 1 and Table 1.

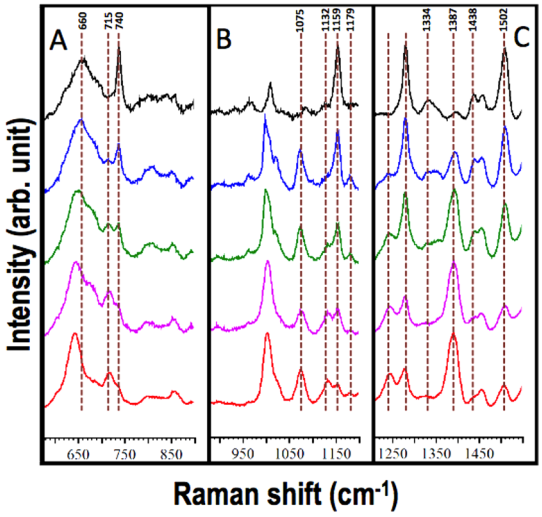

Figure 1. SERS spectra recorded during the exposure of the HaCaT cell DNA with H_2O_2/UV. Various regions showing characteristic SERS bands of DNA are shown in panels A−C. From top to bottom: SERS spectra recorded at 0, 5, 10, 15, and 20 min.

TABLE 1. Assignment of Bands in SERS Spectra of HaCaT Cell DNA before and after ROS Attack[a]

before ROS attack (cm^{-1})	after ROS attack (cm^{-1})	tentative assignments of SERS bands
660	640	dG
740	715⊥738	RB dA and dT
800	800	ν(O−P−O)
1085	1075↓	PO^{2-} sym. stretch, bk
1159	1159↓	dA
1179	1179↑	dT
1334	1334↓	dA
1387	1387↑	dA, dT, and dG
1438	1438↓	dT
1502	1502↓	dG and dA

[a] dA, deoxyadenosine; dG, deoxyguanosine; dT, deoxythymidine; bk, backbone; sym, symmetric. ⊥ = Splitting of SERS bands. ↑ = Increase in SERS intensity. ↓ = Decrease in SERS intensity.

Because of the high reactivity, hydroxyl radicals are expected to abstract the hydrogen atoms from the sugar−phosphate backbone, especially C5′-H and C4′-H, as these are the most solvent-exposed hydrogen atoms in the DNA backbone.[27] This may lead to the β-cleavage and strand breakage followed by release of an altered sugar and an intact base.[28,29] Raman bands in the region 800−1100 cm^{-1} are generally sensitive to backbone geometry and secondary structure of DNA.[30] The phosphate backbone confirmation marker found at 1085 cm^{-1} was drastically increased in its intensity and was shifted to 1075 cm^{-1} just after 5 min of exposure to H_2O_2/UV, which can be attributed to the scissions of double- or single-stranded DNA followed

by the aggregation of DNA as a result of hydrogen atom abstraction by the ROS. This was supported by the data obtained from the detailed analysis of the regions corresponding to the Raman marker bands of nucleobases. In fact, the adenine ring breathing (RB) band and thymidine marker band in native DNA were merged together and appeared as a single band at 740 cm^{-1} (Figure 1A). It is known that an increase in Raman intensities often occurs when DNA bases become unstacked.[30] As a remarkable consequence of ROS-induced backbone damage and base unstacking, the band observed at 740 cm^{-1} split into two distinct bands and was found at 715 and 738 cm^{-1} after 10 min, which can be attributed to unpaired adenosine and thymidine residues, respectively. The intensity of thymidine residue was further reduced after 20 min of exposure, possibly because of the formation of various photoproducts of dT, as exposure of UV light can result in the formation of lesions such as cyclobutane pyrimidine dimers (CPD), (6−4) photoproducts, *etc.*[31]

The abstraction of hydrogen atoms from the sugar−phosphate backbone by the ROS and subsequent damage to the native DNA backbone can induce the destabilization of DNA duplex and can lead to the rupturing of hydrogen bonds and the base pairs to swing open.[30] This may lead to the formation of many unpaired base residues. These base residues can get chemically modified by the attack of free radicals and may form many lesions. Among them 8-oxoguanosine is the most common lesion, as guanine is more prone to oxidation compared to other DNA bases.[32,33] Normally, the RB band of guanine may vary from 600 to 700 cm^{-1}, which is dependent on the sugar-base conformation.[15,34] The band observed at ~660 cm^{-1} (mainly constitutes to the RB vibration of guanine) shifted toward the lower wavenumber side with time upon exposure to H_2O_2/UV. This shift has been previously assigned to presence of oxidized base lesions and their ability to make sharp bends or kinks, which in turns makes the modification in the DNA conformation and leads to deformation around the lesion sites by disruption of base-stacking in DNA duplex at the lesion sites. This can reduce the force constant for their bending that can ultimately reflect in the frequency of Raman vibrations.[24] The RB vibration of guanine is sensitive to its orientation relative to the ribose ring structure and may be a useful reporter for the presence of chemical modifications.[34] It was also noticed that the vibration of dA at 1159 cm^{-1} showed a decrease in its intensity with a simultaneous emergence of a new band at 1179 cm^{-1} after 5 min of exposure. This new band has been attributed to the vibration and corresponds to unpaired dT. It has been reported that the intensity of this vibration diminishes when unpaired dT becomes paired with dA.[35] However, the intensity of this Raman band further diminished with time, possibly because of the formation of various photoproducts of dT.[31]

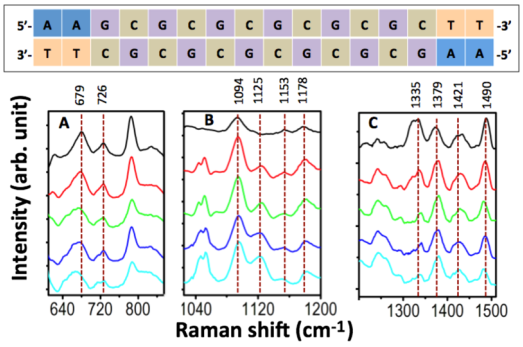

Figure 2. SERS spectra recorded during the reaction of synthetic DNA (AAG) with H_2O_2/UV. The sequence of AAG is also given. Various regions showing characteristic SERS bands of DNA are shown in panels A−C. From top to bottom: SERS spectra recorded at 0, 5, 10, 15, and 20 min.

Interestingly, we noted that the ratio between the intensities of vibration observed at 1387 cm^{-1} (from dA, dT, and dG) and 1334 cm^{-1} (from dA), (I_{1387}/I_{1334}), increased with respect to time, which is directly related to the extent of aggregation of DNA.[30] The aggregation can lead to a perturbation of the local environment around the purine bases, which may help the free radicals to attack the newly exposed base sites. Since the base oxidation is relatively more time-consuming than the backbone degradation, it reflected as a sudden modification in the SERS band of phosphate backbone stretching vibration within 5 min, whereas modification in the RB vibration of guanosine due to its oxidation happened over a period of 20 min. Apart from this, an obvious modification in the conformation of the DNA was suggested by the reduction in the intensity of the band assigned to the phosphate diester symmetric stretching found in between 790 and 830 cm^{-1}.

We noticed a sharp decrease in the intensity of C5′-H2 deformation band of thymine found at 1438 cm^{-1} during the course of free radical attack, which shows the perturbations of the deoxyribonucleoside conformation of A−T base pairs due to the deformation in thymidine moiety[36] (note that a similar reduction in the intensity was found in the combination band of adenine and thymine at 740 cm^{-1}). A decrease in the Raman band (at 1458 cm^{-1}) of deoxyribose moieties (with a small contribution from adenine vibrations)[37] was also apparent in the spectrum. The reduction in the intensity also suggests the modification in the backbone and chemical modifications in adenine. Apart from this, as a consequence of oxidation of guanosine by the attack of free radicals, the SERS band corresponds to guanine and adenine with more contribution from guanine,[38,39] found at 1502 cm^{-1}, and also decreased in its intensity.

In order to get more detailed information on ROS-induced modifications in the Raman features of DNA, SERS experiments for small chain length DNA have been conducted. For this study, dsDNA-AAG was used. The sequence of AAG is given in Figure 2. As in the case of genomic DNA, the RB vibration band of guanine

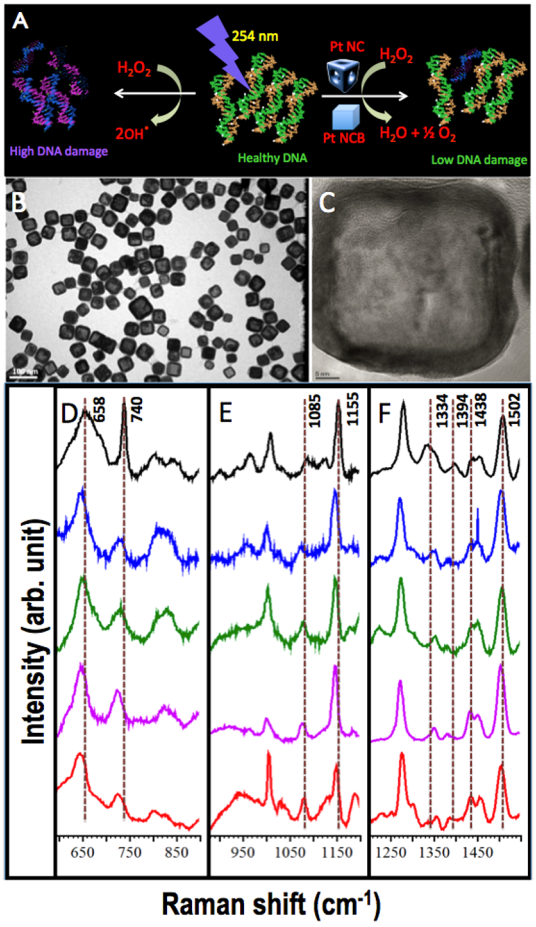

Figure 3. (A) Schematic showing the fate of HaCaT DNA during the UV photolysis of H_2O_2 in presence and absence of Pt nanoparticles. (B) and (C) are the large area and single particle TEM images of Pt NCs, respectively. (D–F) SERS spectra recorded during the reaction of HaCaT cell DNA with H_2O_2/UV in presence of Pt NCs. Various regions showing characteristic SERS bands of DNA are shown in panels D–F. From top to bottom: SERS spectra recorded at 0, 5, 10, 15, and 20 min.

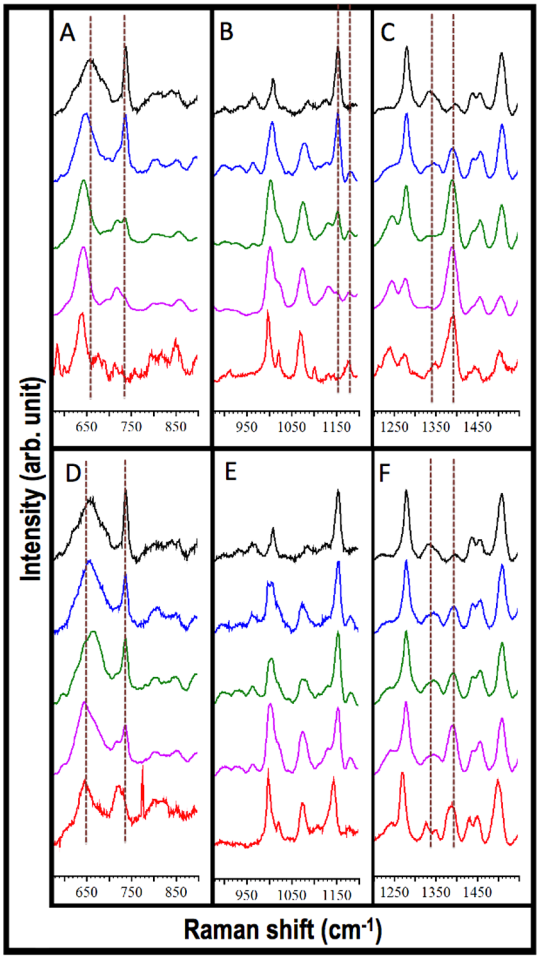

Figure 4. SERS spectra recorded during the reaction of HaCaT cell DNA with Fenton's reagent in absence (A–C) and presence (D–F) of Pt NCs. From top to bottom: SERS spectra recorded at 0, 5, 10, 15, and 20 min.

observed at ~679 cm^{-1} shifted gradually toward the lower wavenumber (~660 cm^{-1}) with time upon treatment with Fenton's reagent (Figure 2), and the adenine RB vibration (726 cm^{-1}) split into two bands (725 and 718 cm^{-1}). Apart from this, a sudden increase in the phosphate backbone vibration was also observed after 5 min. SERS bands correspond to aggregation of DNA, which was obvious in the spectra (Figure 2C). Full SERS spectra for these events have been given in Figure S1 (Supporting Information). These results were also in concordance with the results obtained for genomic DNA.

Even though several nanoparticles are well-known for their free radical scavenging activity, platinum nanoparticles have been considered as excellent antioxidants because of their good biocompatibility and unique catalytic activity.[4,5] Here, we monitored the effectiveness of various Pt nanoparticles in preventing the DNA damage caused by the ROS with the help of SERS. For this study, we used Pt nanocages (Pt NCs) and nearly cubical Pt nanoparticles (Pt NCBs). To investigate antioxidant activity of Pt nanoparticles, 1 nM solution of Pt NCs (45–50 nm) was incubated with H_2O_2 for about 5 min prior to UV light exposure, which was then mixed with HaCaT cell DNA and Ag NPs (5 nM). SERS spectra from this mixture were collected in a time-dependent manner while it was being exposed to UV light. From the SERS spectra of DNA treated with H_2O_2/UV in presence of Pt NCs, we indeed observed a reduction in the DNA damage (Figure 3). Even after 30 min, though the band observed at 740 cm^{-1} shifted to ~723 cm^{-1}, no splitting was observed, suggesting the absence of any severe hydrogen bond rupturing between the A–T base pairs. Apart from that, no drastic shift was observed in the guanine RB band at 658 cm^{-1} band as a function of time, probably because of the absence of any severe oxidative damage to guanine in presence of Pt NCs. The above facts indicate that scissions of double- or single-stranded DNA or oxidation of nucleobases have been reduced to a large extent in presence of Pt NCs. The SERS band corresponding to the

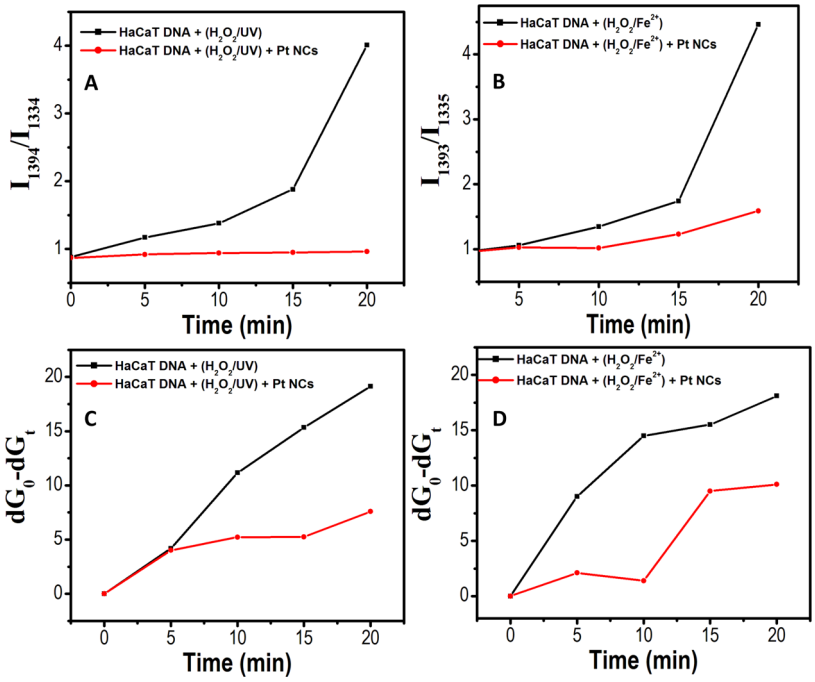

Figure 5. Plots showing extent of DNA aggregation (A and B) and chemical modifications in the guanine RB band (C and D) during ROS-induced DNA damage when DNA was exposed to H_2O_2/UV (A and C) and when DNA was treated with Fenton's reagent (B and D).

phosphate backbone confirmation marker found at 1085 cm^{-1} remained almost unchanged, despite being the most susceptible bond for free radical attack (Figure 3). This is pointing toward the fact that Pt NCs retard the process of possible hydrogen abstraction from the sugar−phosphate backbone by the ROS. We also noted that the ratio between the bands found at 1394 and 1334 cm^{-1} (I_{1394}/I_{1334}) did not show any drastic changes even after 20 min, which indicates an obvious absence of free radical-induced backbone damage and subsequent aggregation. The ROS degradation capability of Pt NCs can be attributed to the following reasons. Pt nanoparticles are known for their catalase-like activity in converting hydrogen peroxide to water and oxygen by the two-electron oxidation/reduction reaction (Figure 3A).[4,40] We believe that the cage-effect may also play an important role in the efficiency of free radical scavenging activity of Pt NCs.[41,42] Trace amounts of Ag present in Pt NCs (since Pt NCs are prepared from Ag NCBs as template) may also enhance the degradation reaction of H_2O_2, as bimetallic nanoparticles of Pt are known for their enhanced and tunable catalytic activity.[43]

Although H_2O_2 is not a strong reactive species, the traces of copper and iron present inside the cells are capable of catalyzing the free-radical reactions to generate highly reactive hydroxyl radicals through a Fenton's reaction.[44,45] In order to further investigate the free radical scavenging ability of Pt NCs toward the free radicals generated *via* Fenton's reaction, the HaCaT cell DNA was treated with Fe^{2+}/H_2O_2 as explained in the Experimental Methods.

The SERS spectra were collected in a time-dependent manner in presence and absence of Pt NCs, while the DNA was treated with Fenton's reagent. As in the case of DNA damage caused by the exposure to H_2O_2/UV, considerable modifications were found in the SERS spectra of the DNA after treating them with Fenton's reagent (Figure 4A−C), whereas addition of Pt NCs protected the DNA from the attack of hydroxyl radicals generated by the Fenton's reaction to a large extent, which resulted in the retention of its native form (Figure 4D−F). However, the SERS spectra of DNA exposed to Fenton's reagent in presence of Pt NCs also showed features of aggregation even after 5 min. Specifically, the ratio between the intensities of the Raman bands at I_{1393} and I_{1335} (I_{1393}/I_{1335}) showed a value greater than 1. This was absent in the SERS spectra of DNA exposed to H_2O_2/UV after 5 min. The graph plotted between the ratio of intensities between band at 1394 and 1334 cm^{-1} clearly depicts this (Figure 5A). This can be due to the metal ion-induced aggregation usually found in DNA as a result of Fe^{2+} ions in Fenton's reagent.[30] The hydroxyl radical generated by Fenton's reagent can attack DNA and cause single- or double-stranded breaks. This was evident from the SERS spectra of the DNA exposed to the ROS in the absence of Pt NCs (Figure 4A−C). Absence of any drastic modification in the characteristic Raman bands corresponding to the sugar phosphate backbone and nucleobase ring vibrations even after 15 min (Figure 4D−F) of ROS exposure, in presence of Pt NCs, indicates that the decomposition of H_2O_2 proceeds *via* a two-electron redox reaction, ruling out the

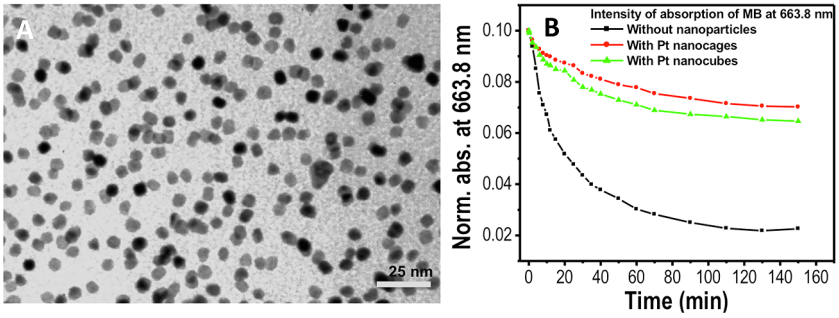

Figure 6. (A) TEM image of Pt NCBs. (B) Kinetic curves of Fenton's reagent-induced decoloration of MB in presence of Pt NCs and Pt NCBs.

possibility of formation of any hydroxyl radical.[40] Apart from this a significant amount of Fe^{2+} in the Fenton's reagent could also be converted into Fe^{3+} by the catalytic oxidation of Fe^{2+} on Pt nanoparticle surfaces, which may further reduce the possibility of formation of hydroxyl radicals by one electron redox reaction pathway.[5]

The phosphate backbone confirmation marker found at 1082 cm^{-1} and the band corresponding to the RB vibration of guanosine (658 cm^{-1}) showed an immediate change in its peak position revealing that Fenton's reagent can induce phosphate backbone rupture and nucleobase oxidation instantaneously (Figure 4).

As in the case of H_2O_2/UV induced damage, the band at 739 cm^{-1} also showed almost the same trend after treatment with Fenton's reagent. This suggests the possible rupturing of the hydrogen bond between the base pair dA−dT. On the contrary to the DNA damage caused by H_2O_2/UV exposure, the guanine RB band showed a sudden and noticeable shift that was evident from Figure 4A and the graph shown in Figure 5C,D. This indicates that Fenton's reagent is more powerful toward the quick oxidation of the nucleobases compared to the H_2O_2/UV exposure. The vibration of adenosine at 1158 cm^{-1} also showed a similar trend as in the case of damage caused by H_2O_2/UV. The intensity of this vibration decreased with a simultaneous emergence of a new band due to dT at 1178 cm^{-1} after 5 min of exposure. However, the intensity of this band did not diminish even after 20 min since there is no possibility of formation of any photoproducts.

Shape of the nanoparticles is known to play a vital role in its catalytic activity.[46] To study the shape effects on H_2O_2 decomposition by Pt nanoparticles, we extended our study to nearly cubical Pt nanoparticles (Pt NCBs). The TEM analysis shows that these nanoparticles are nearly cubical in shape (with spheres and truncated particles), with an average size of 10 nm (Figure 6A). The effectiveness of Pt NCBs in preventing ROS-induced DNA damage was monitored in real time by using SERS (Figure 7). As in the case of Pt NCs, substantial reduction in the DNA damage was also shown by 1 nM of Pt NCBs against the ROS generated *via* UV photolysis of H_2O_2. The vibration band corresponding to the phosphate backbone (1078 cm^{-1}) remained

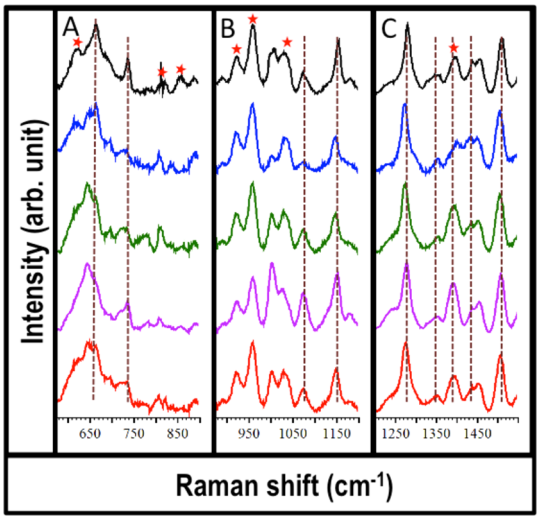

Figure 7. SERS spectra recorded during the reaction of HaCaT cell DNA with H_2O_2/UV in presence of Pt NCBs. Various regions showing characteristic SERS bands of DNA are shown in panels A−C. From top to bottom: SERS spectra recorded at 5, 10, 15, 20, and 30 min. The Raman bands marked by stars are indicating the possible contribution from the PVP ligand present on the Pt NCBs.

almost unaltered, ruling out the possibility of any severe single or double strand break. The Raman markers bands corresponding to the nucleobase vibrations remained unchanged without any drastic modification. Because of the small size of Pt NCBs, we could not remove the PVP ligand completely from the samples. Hence, vibrations corresponding to PVP appeared in the SERS spectra (see Figure S2, Supporting Information). Apparently, these vibrations were easily distinguishable and are marked in the spectra (Figure 7).

In order to study the effectiveness of H_2O_2 degradation by various Pt nanoparticles, a kinetic investigation of Pt-catalyzed degradation of methylene blue (MB) by the Fenton's reagent was performed by measuring the absorbance at 663.8 nm as a function of time after adding different Pt nanoparticles. Here, H_2O_2 was mixed with Pt nanoparticles for 5 min prior to the addition of MB and Fe^{2+}. The UV−vis absorption spectra collected at different time intervals of the degradation reactions are shown in Figure S3 (Supporting Information). From the plot of absorbance *versus* time at 663.8 nm, a distinct reduction

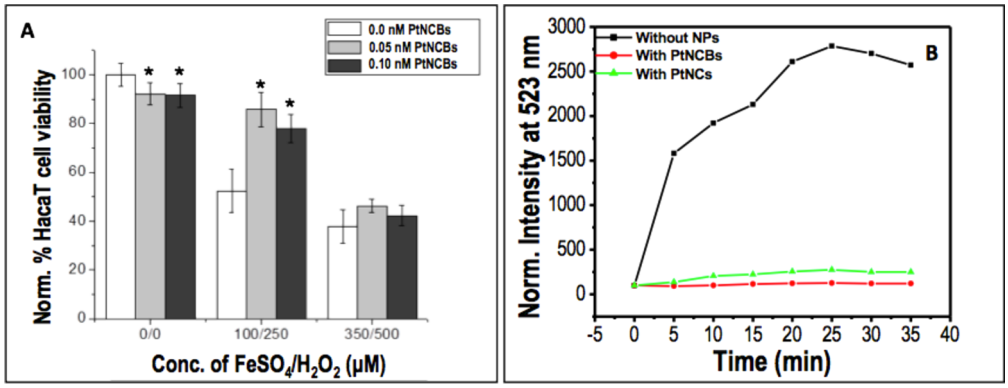

Figure 8. (A) Cell viability results for the HaCaT cells treated with Pt NCBs (0.05 and 0.1 nM) in presence of 100 μM $FeSO_4$/250 μM H_2O_2 and 350 μM $FeSO_4$/500 μM H_2O_2. Statistically significant data (comparing Pt NCB treatments to no Pt NCB treatment) is indicated by * (*p*-value < 0.05). (B) Plot showing the fluorescence intensity of the compound formed by the interaction of DCF and ROS as a function of time. The data were collected in presence and absence of Pt nanoparticles.

in the rate of MB degradation in presence of both Pt NCs and Pt NCBs are observed (Figure 6B). However, calculation of the magnitude of ROS degrading capability of the former was severely hampered because of the limitation in calculating the exact number of Pt atoms in the Pt NCs.

We extended our study to understand the cell viability and ROS degradation activity of various Pt nanoparticles in HaCaT cells. HaCaT cells were grown overnight in a 96-well tissue culture plate, after which they were treated with Pt nanoparticles (0.05 and 0.1 nM) in the presence of 100 μM $FeSO_4$/250 μM H_2O_2 and 350 μM $FeSO_4$/500 μM H_2O_2 for 24 h. The cell viability assay was carried out using XTT. Among the Pt nanoparticles, Pt NCBs did not show any toxic effect on the HaCaT cells (~90% cell viability at 0.05 and 0.1 nM) and also showed significant antioxidant activity (Figure 8), especially in the case of 0.05 nM Pt NCBs with 100 μM $FeSO_4$/250 μM H_2O_2. As bare Pt NCs (at 0.05 and 0.1 nm) itself showed toxic effect to the HaCaT cells (Figure S4, Supporting Information), we could not compare the efficiency in this context. As we used bare Pt NCs for this study, the observed toxicity at these concentrations could be attributed to the presence of residual amount of Ag present in it, as the Pt NCs were synthesized from Ag nanocube through galvanic replacement reaction. At the same time, ICP analysis did not show the presence of any Ag in the cleaned Pt NCB samples.

Furthermore, the ROS-degrading activity of Pt nanoparticles was confirmed by 2′,7′-dichlorofluorescein (DCF) assay. For the DCF assay, we used 2′,7′-dichlorofluorescein diacetate (DCFDA), a fluorogenic dye that measures amount of ROS. Here, DCFDA is deacetylated to a nonfluorescent compound (in alkaline medium). Further, this compound was allowed to react with Fenton's reagent to convert it into highly fluorescent 2′,7′-dichlorofluorescin. The resultant compound was detected by fluorescence spectroscopy, which showed an excitation maximum at ~493 nm and emission at ~523 nm (spectra given in Figure S5, Supporting Information). We found that the rate of conversion of nonfluorescent DCFDA to fluorecent DCF is very low in the presence of the Pt nanoparticle (Figure 8B and Figure S6, Supporting Information), because of the degradation of H_2O_2 in the Fenton's reagent by the Pt nanoparticles.

CONCLUSION

The potential of SERS in direct observation of ROS-induced damages in the HaCaT cell DNA was demonstrated. A multitude of chemical and physical changes within DNA caused by ROS generated *via* Fenton's reaction and UV photolysis of H_2O_2 were monitored using SERS in real time. In addition to this, the ability of Pt nanoparticles to prevent ROS-induced oxidative damage to cellular DNA was assessed using SERS, which showed a reduction in prompt DNA aggregation, backbone damage, and residual damage to the DNA bases. Such materials would possibly find application in developing chemopreventive drugs against many ROS-induced deceases. The antioxidant activity of the Pt nanoparticles was further confirmed by using DCF assay and cell viability studies. Our findings open up the immense possibilities of SERS in diagnosing various stages of a multitude of diseases, especially cancer.

EXPERIMENTAL METHODS

Preparation of Citrate Capped Ag Nanoparticles (Ag NPs). Ag NPs were prepared according to Turkevich method.[47] Briefly, 75 mg sodium citrate dissolved in 1 mL of deionized (DI) water was added dropwise to a boiling solution of 5 mM $AgNO_3$ in 50 mL of DI water. Heating was continued for a few more minutes, and then the suspension was cooled rapidly in an ice bath. Later, 10 mL of the as prepared Ag NPs solution was centrifuged, and the residue after washing with distilled water was redispersed in 500 μL of DI water. These Ag NPs solution showed surface plasmon resonance peak at 420 nm, which is characteristic of silver nanoparticles.

Synthesis of Pt Nanocages. Pt nanocages (Pt NCs) were prepared from silver nanocubes (Ag NCBs) by galvanic replacement of silver atoms by platinum following our earlier procedure.[41] In a typical synthesis of Ag NCBs, 35 mL of ethylene glycol (EG) was heated at 150 °C for 1 h. To this solution, 0.25 g of poly(vinyl pyrrolidone) (PVP, MW ~ 55 000) dissolved in 5 mL of EG was added followed by 0.4 mL of sodium sulfide (3 mM) in EG. Addition of ethylene glycol solution of $AgNO_3$ (0.12 g in 5 mL) to the above solution resulted in the formation of Ag NCBs after 15 min. These Ag NCBs were cleaned by washing them with water−acetone mixture followed by centrifugation at 14000 rpm for 10 min. The residue containing Ag NCBs was redispersed in 20 mL of DI water and used for further experiments. Two milliliters of this Ag NCBs solution was then transferred to a 30 mL vial, which was further diluted with 20 mL of DI water. An aqueous solution of potassium tetrachloroplatinate(II) (K_2 $PtCl_4$) of a concentration of 0.05 g/10 mL was added to the above solution (0.5 mL/5 min) with constant shaking. Afterward, a dilute solution of K_2PtCl_4 (0.005 g/10 mL of DI water) was added (0.5 mL/5 min) to the reaction mixture until the solution turned black. Pt NCs thus obtained were cleaned using a similar procedure as Au NCBs.

Synthesis of Nearly Cubical Pt Nanoparticles. In a typical synthesis of nearly cubical Pt nanoparticles (Pt NCBs), 30 mL of EG was heated under stirring in a 50 mL round-bottom flask at 140 °C for 30 min in an oil bath. An amount of 1 g of PVP (MW ~ 55 000) was added, and the temperature was raised to 155 °C. Then, 1 mL of $AgNO_3$ solution (0.017 g $AgNO_3$ dissolved in 10 mL of EG) was added followed by 0.2 mL of chloroplatinic acid hydrate solution from 5 mL of stock solution (0.3 g/5 mL of EG). Afterward, the temperature was raised to 180 °C, and the rest of the platinum solution was added drop by drop. The resultant solution was stirred and heated for 20 min. The platinum nanoparticles were cleaned by mixing 1 mL of the as prepared solution with 1 mL of acetone and then centrifuged at 15000 rpm for 30 min. The residue was redispersed in 1 mL of DI water and was used for further studies.

An axial inductively coupled plasma (ICP) atomic emission spectrometer machine was used to determine the concentration of all the nanoparticles solutions. A minimum of three ICP measurements was taken for each sample.

Cell Culture. Human keratinocytes (HaCaT) were maintained in Dulbecco's modified Eagles' medium (DMEM, Mediatech) supplemented with 10% v/v fetal bovine serum (FBS, Mediatech) and 1% antimycotic solution (Mediatech) in a 37 °C, 5% CO_2 humidified incubator.

Cell Viability Assay. HaCaT cells were plated in a 96-well tissue culture plate and allowed to grow for 24 h. The culture medium was then removed and replaced with culture medium containing the Fenton's reagent and/or Pt nanoparticles at varying concentrations. Cells were incubated with treatment for 24 h. After that the cells were washed with PBS and the XTT cell viability assay kit (Biotium, Inc.) according to the manufacturer's protocol. The cell viabilities of the treated cells were normalized to the control (HaCaT cells treated with culture medium only). The error bar is expressed as ± the percent relative standard deviation (% rsd). Statistical significance (p-value) was calculated by a t test calculator (GraphPad Software, Inc.). Data is considered statistically significant when $p < 0.05$.

DNA Isolation. Genomic DNA was isolated by using an extraction procedure described earlier.[48] Briefly, the cells were lysed with 4 mL of lysis buffer containing 0.5 M Tris-HCl (pH 8.0), 20 mM EDTA, 10 mM NaCl, 1% SDS, and 0.5 mg/mL proteinase K. This was incubated overnight at 55 °C. Subsequently, 2 mL of saturated NaCl (~6 M) was added, and the samples were incubated at 55 °C for 10 min. After centrifugation at 5000 rpm for 30 min, the supernatant containing DNA was mixed with 2 volumes of prechilled ethanol (100%), and the DNA was spooled by gently inverting the mix. The tubes were incubated at room temperature for 15 min, and the DNA was recovered by centrifuging at 10000 rpm for 10 min at room temperature. The DNA was washed several times thoroughly with 70% ethanol. The tubes were placed inverted on benchtop and allowed to air-dry at ambient conditions. Required amount of DNA was dissolved in DI water and was used for the SERS analysis.

Assay for Reactive Oxygen Species Using 2′,7′-Dichlorofluorescein (DCF). DCF was prepared from 2′,7′-dichlorofluorescein diacetate (DCFDA) by mixing 0.5 mL of 1.0 mM DCFDA in methanol with 2.0 mL of 0.01 N NaOH. This de-esterification process of DCFDA has been continued at 27 °C for 30 min. The resultant mixture was then neutralized with 10 mL of 25 mM NaH_2PO_4 and kept on ice bath in the dark until use. The assay was carried out at 27 °C by adding 100 μL of DCF (1 mM) to the Fenton's reagent (H_2O_2 (100 μM) + Fe^{2+} (100 μM)). The experiments were also performed in presence of 25 μL of 1 nM Pt nanoparicles.

SERS Measurements. For the SERS investigation of ROS-induced modification in the genomic DNA, 8.824×10^3 μM of H_2O_2 was added to a mixture of solution containing DNA (0.1 mg/1 mL) and Ag nanoparticle solution (5 nM). The SERS spectra were collected in a time-dependent manner in presence and absence of Pt NCs, while the DNA was being exposed to UV light (254 nm). To investigate the free radical scavenging ability of Pt nanoparticles toward the free radicals generated *via* Fenton's reaction, oxidation of DNA was carried out by treating them with Fenton's reagent.[49] Briefly, a solution of DNA (0.1 mg/1 mL) was mixed with Fenton's reagent (50 μM of Fe^{2+} and 14.706×10^3 μM of H_2O_2), and time-dependent SERS spectra were collected directly from the suspension in presence and absence of Pt nanoparticles. For all the experiments, Pt nanoparticles of concentration 1 nM have been used. Throughout the SERS measurements we gave special attention to prevent dehydration-induced conformational modifications to the DNA. A similar experiment was conducted with double stranded (ds) DNA of sequence 5′-AAGCGCGCGCGCTT-3′ (this sample is named as "AAG"). The synthetic DNA samples were purchased from Sigma-Aldrich, USA. For all the measurements, the DNA-Ag colloid solution was placed on a Si wafer, and the SERS spectra were measured with a 1800 lines/mm grating using a Renishaw InVia Raman spectrometer (with a spectral resolution of ~1 cm^{-1}) coupled to a Leica microscope. The laser (532 nm) was directed into a microscope *via* a series of reflecting lenses and apertures, where it was focused onto the sample by a 50× objective. The backscattered signals from the samples were collected by a CCD detector in the range of 400 to 2000 cm^{-1}. The spectra were processed by removal of the spectral background. Here, cubic spline interpolation is used for the baseline fit by manually selecting the points representative of the background.

Conflict of Interest: The authors declare no competing financial interest.

Acknowledgment. We thank National Science Foundation (NSF) for constantly supporting our research program. This work was supported by NSF-DMR Grant (1206637). Justin Bordley is thanked for help with the TEM measurements.

Supporting Information Available: Additional SERS data, UV−vis spectra of Fenton's reagent-induced decoloration of MB in presence of Pt NCs and Pt NCBs, cell viability data, fluorescence spectra for DCF assay. This information is available free of charge *via* the Internet at http://pubs.acs.org.

REFERENCES AND NOTES

1. Hussain, S. P.; Hofseth, L. J.; Harris, C. C. Radical Causes of Cancer. *Nat. Rev. Cancer* **2003**, *3*, 276–285.
2. Yin, H.; Xu, L.; Porter, N. A. Free Radical Lipid Peroxidation: Mechanisms and Analysis. *Chem. Rev.* **2011**, *111*, 5944–5972.
3. Ingold, K. U.; Bowry, V. W.; Stocker, R.; Walling, C. Autoxidation of Lipids and Antioxidation by Alpha-Tocopherol and Ubiquinol in Homogeneous Solution and in Aqueous Dispersions of Lipids: Unrecognized Consequences of Lipid Particle Size as Exemplified by Oxidation of Human Low Density Lipoprotein. *Proc. Natl. Acad. Sci. U. S. A.* **1993**, *90*, 45–49.
4. Kajita, M.; Hikosaka, K.; Iitsuka, M.; Kanayama, A.; Toshima, N.; Miyamoto, Y. Platinum Nanoparticle is a Useful Scavenger of Superoxide Anion and Hydrogen Peroxide. *Free Radical Res.* **2007**, *41*, 615–626.

5. Aki, W.; Masashi, K.; Juewon, K.; Atsuhiro, K.; Kyoko, T.; Tadahiko, M.; Yusei, M. *In Vitro* Free Radical Scavenging Activity of Platinum Nanoparticles. *Nanotechnology* **2009**, *20*, 455105.
6. Tsai, Y.-Y.; Oca-Cossio, J.; Lin, S.-M.; Woan, K.; Yu, P.-C.; Sigmund, W. Reactive Oxygen Species Scavenging Properties of ZrO_2−CeO_2 Solid Solution Nanoparticles. *Nanomedicine* **2008**, *3*, 637–645.
7. Yamashita, N.; Murata, M.; Inoue, S.; Burkitt, M. J.; Milne, L.; Kawanishi, S. α-Tocopherol Induces Oxidative Damage to DNA in the Presence of Copper(II) Ions. *Chem. Res. Toxicol.* **1998**, *11*, 855–862.
8. Bruner, S. D.; Norman, D. P. G.; Verdine, G. L. Structural Basis for Recognition and Repair of the Endogenous Mutagen 8-Oxoguanine in DNA. *Nature* **2000**, *403*, 859–866.
9. Bhattacharjee, S.; Chatterjee, S.; Jiang, J.; Sinha, B. K.; Mason, R. P. Detection and Imaging of the Free Radical DNA in Cells—Site-Specific Radical Formation Induced by Fenton Chemistry and its Repair in Cellular DNA as Seen by Electron Spin Resonance, Immuno-Spin Trapping and Confocal Microscopy. *Nucleic Acids Res.* **2012**, *40*, 5477–5486.
10. Chatgilialoglu, C.; Ferreri, C.; Terzidis, M. A. Purine 5′,8-Cyclonucleoside Lesions: Chemistry and Biology. *Chem. Soc. Rev.* **2011**, *40*, 1368–1382.
11. Dizdaroglu, M.; Bergtold, D. S. Characterization of Free Radical-Induced Base Damage in DNA at Biologically Relevant Levels. *Anal. Biochem.* **1986**, *156*, 182–188.
12. Zhou, L.; Yang, J.; Estavillo, C.; Stuart, J. D.; Schenkman, J. B.; Rusling, J. F. Toxicity Screening by Electrochemical Detection of DNA Damage by Metabolites Generated *in Situ* in Ultrathin DNA−Enzyme Films. *J. Am. Chem. Soc.* **2003**, *125*, 1431–1436.
13. Furman, J. L.; Mok, P.-W.; Badran, A. H.; Ghosh, I. Turn-On DNA Damage Sensors for the Direct Detection of 8-Oxoguanine and Photoproducts in Native DNA. *J. Am. Chem. Soc.* **2011**, *133*, 12518–12527.
14. Benevides, J. M.; Wang, A. H.-J.; Thomas, G. J. Demonstration of Z-d(5BrCGAT5BrCG) and B-d(CGCGATCGCG) Form Crystal Stuctures in DNA-Cobalt Hexammine Complexes by Kr 647.1 nm Excitation of Raman Spectra. *Nucleic Acids Res.* **1993**, *21*, 1433–1438.
15. Pagba, C. V.; Lane, S. M.; Wachsmann-Hogiu, S. Conformational Changes in Quadruplex Oligonucleotide Structures Probed by Raman Spectroscopy. *Biomed. Opt. Express* **2011**, *2*, 207–217.
16. Sánchez, V.; Redmann, K.; Wistuba, J.; Wübbeling, F.; Burger, M.; Oldenhof, H.; Wolkers, W. F.; Kliesch, S.; Schlatt, S.; Mallidis, C. Oxidative DNA Damage in Human Sperm Can Be Detected by Raman Microspectroscopy. *Fertil. Steril.* **2012**, *98*, 1124–1129.
17. Ahijado-Guzmán, R.; Gómez-Puertas, P.; Alvarez-Puebla, R. A.; Rivas, G.; Liz-Marzán, L. M. Surface-Enhanced Raman Scattering-Based Detection of the Interactions between the Essential Cell Division FtsZ Protein and Bacterial Membrane Elements. *ACS Nano* **2012**, *6*, 7514–7520.
18. Mathew, A.; Panikkanvalappil, S. R.; Pradeep, T. Selective Visual Detection of TNT at the Sub-Zeptomole Level. *Angew. Chem., Int. Ed.* **2012**, *51*, 9596–9600.
19. Braun, G.; Lee, S. J.; Dante, M.; Nguyen, T.-Q.; Moskovits, M.; Reich, N. Surface-Enhanced Raman Spectroscopy for DNA Detection by Nanoparticle Assembly onto Smooth Metal Films. *J. Am. Chem. Soc.* **2007**, *129*, 6378–6379.
20. Lu, W.; Singh, A. K.; Khan, S. A.; Senapati, D.; Yu, H.; Ray, P. C. Gold Nano-Popcorn-Based Targeted Diagnosis, Nanotherapy Treatment, and *in Situ* Monitoring of Photothermal Therapy Response of Prostate Cancer Cells Using Surface-Enhanced Raman Spectroscopy. *J. Am. Chem. Soc.* **2010**, *132*, 18103–18114.
21. Sha, M. Y.; Xu, H.; Natan, M. J.; Cromer, R. Surface-Enhanced Raman Scattering Tags for Rapid and Homogeneous Detection of Circulating Tumor Cells in the Presence of Human Whole Blood. *J. Am. Chem. Soc.* **2008**, *130*, 17214–17215.
22. Papadopoulou, E.; Bell, S. E. J. Label-Free Detection of Single-Base Mismatches in DNA by Surface-Enhanced Raman Spectroscopy. *Angew. Chem., Int. Ed.* **2011**, *50*, 9058–9061.
23. Johnson, R. P.; Richardson, J. A.; Brown, T.; Bartlett, P. N.; Label-Free, A. Electrochemical SERS-Based Assay for Detection of DNA Hybridization and Discrimination of Mutations. *J. Am. Chem. Soc.* **2012**, *134*, 14099–14107.
24. Panikkanvalappil, S. R.; Mackey, M. A.; El-Sayed, M. A. Probing the Unique Dehydration-Induced Structural Modifications in Cancer Cell DNA using Surface Enhanced Raman Spectroscopy. *J. Am. Chem. Soc.* **2013**, *135*, 4815–4821.
25. Emen, S.; ceken, B.; I, G.; I, M. DNA Damage Protecting Activity and *in Vitro* Antioxidant Potential of the Methanol Extract of Cyclotrichium Niveum. *Pharm. Biol.* **2009**, *47*, 219–229.
26. Maynard, S.; Swistowska, A. M.; Lee, J. W.; Liu, Y.; Liu, S.-T.; Da Cruz, A. B.; Rao, M.; de Souza-Pinto, N. C.; Zeng, X.; Bohr, V. A. Human Embryonic Stem Cells Have Enhanced Repair of Multiple Forms of DNA Damage. *Stem Cells* **2008**, *26*, 2266–2274.
27. Balasubramanian, B.; Pogozelski, W. K.; Tullius, T. D. DNA Strand Breaking by the Hydroxyl Radical is Governed by the Accessible Surface Areas of the Hydrogen Atoms of the DNA Backbone. *Proc. Natl. Acad. Sci. U. S. A.* **1998**, *95*, 9738–9743.
28. Beesk, F.; Dizdaroglu, M.; Schulte-Frohlinde, D.; Von Sonntag, C. Radiation-Induced DNA Strand Breaks in Deoxygenated Aqueous Solutions. The Formation of Altered Sugars as End Groups. *Int. J. Radiat. Biol.* **1979**, *36*, 565–576.
29. Aust, A. E.; Eveleigh, J. F. Mechanisms of DNA Oxidation. *Proc. Soc. Exp. Biol. Med.* **1999**, *222*, 246–252.
30. Duguid, J. G.; Bloomfield, V. A.; Benevides, J. M.; Thomas, G. J., Jr. Raman Spectroscopy of DNA-Metal Complexes. II. The Thermal Denaturation of DNA in the Presence of Sr^{2+}, Ba^{2+}, Mg^{2+}, Ca^{2+}, Mn^{2+}, Co^{2+}, Ni^{2+}, and Cd^{2+}. *Biophys. J.* **1995**, *69*, 2623–2641.
31. Sinha, R. P.; Hader, D.-P. UV-Induced DNA Damage and Repair: A Review. *Photochem. Photobiol. Sci.* **2002**, *1*, 225–236.
32. Steenken, S.; Jovanovic, S. V. How Easily Oxidizable Is DNA? One-Electron Reduction Potentials of Adenosine and Guanosine Radicals in Aqueous Solution. *J. Am. Chem. Soc.* **1997**, *119*, 617–618.
33. Cadet, J.; Delatour, T.; Douki, T.; Gasparutto, D.; Pouget, J.-P.; Ravanat, J.-L.; Sauvaigo, S. Hydroxyl Radicals and DNA Base Damage. *Mutat. Res., Genet. Toxicol. Environ. Mutagen.* **1999**, *424*, 9–21.
34. Nishimura, Y.; Tsuboi, M.; Sato, T. Structure-Spectrum Correlations in Nucleic Acids. I. Raman Lines in the 600−700 cm^{-1} Range of Guanosine Residue. *Nucleic Acids Res.* **1984**, *12*, 6901–6908.
35. Movileanu, L.; Benevides, J. M.; Thomas, G. J. Temperature Dependence of the Raman Spectrum of DNA. II. Raman Signatures of Premelting and Melting Transitions of poly(dA)·poly(dT) and Comparison with poly(dA-dT)·poly(dA-dT). *Biopolymers* **2002**, *63*, 181–194.
36. Marzilli, L. G.; Saad, J. S.; Kuklenyik, Z.; Keating, K. A.; Xu, Y. Relationship of Solution and Protein-Bound Structures of DNA Duplexes with the Major Intrastrand Cross-Link Lesions Formed on Cisplatin Binding to DNA. *J. Am. Chem. Soc.* **2001**, *123*, 2764–2770.
37. Ponkumar, S.; Duraisamy, P.; Iyandurai, N. Structural Analysis of DNA Interactions with Magnesium Ion Studied by Raman Spectroscopy. *Am. J. Biochem. Biotechnol.* **2011**, *7*, 135–140.
38. Andrade, P. O.; Bitar, R. A.; Yassoyama, K.; Martinho, H.; Santo, A. M. E.; Bruno, P. M.; Martin, A. A. Study of Normal Colorectal Tissue by FT-Raman Spectroscopy. *Anal. Bioanal. Chem.* **2007**, *387*, 1643–1648.
39. Segers-Nolten, G. M. J.; Sijtsema, N. M.; Otto, C. Evidence for Hoogsteen GC Base Pairs in the Proton-Induced Transition from Right-Handed to Left-Handed Poly(dG-dC)·Poly(dG-dC). *Biochemistry* **1997**, *36*, 13241–13247.
40. Okamoto, H.; Horii, K.; Fujisawa, A.; Yamamoto, Y. Oxidative Deterioration of Platinum Nanoparticle and its Prevention by Palladium. *Exp. Dermatol.* **2012**, *21*, 5–7.

41. Mahmoud, M. A.; Saira, F.; El-Sayed, M. A. Experimental Evidence for the Nanocage Effect in Catalysis with Hollow Nanoparticles. *Nano Lett.* **2010**, *10*, 3764–3769.
42. Weng, G.; Mahmoud, M. A.; El-Sayed, M. A. Nanocatalysts Can Change the Number of Electrons Involved in Oxidation–Reduction Reaction with the Nanocages Being the Most Efficient. *J. Phys. Chem. C* **2012**, *116*, 24171–24176.
43. He, W.; Wu, X.; Liu, J.; Hu, X.; Zhang, K.; Hou, S.; Zhou, W.; Xie, S. Design of AgM Bimetallic Alloy Nanostructures (M = Au, Pd, Pt) with Tunable Morphology and Peroxidase-Like Activity. *Chem. Mater.* **2010**, *22*, 2988–2994.
44. Keyer, K.; Imlay, J. A. Superoxide Accelerates DNA Damage by Elevating Free-Iron Levels. *Proc. Natl. Acad. Sci. U. S. A.* **1996**, *93*, 13635–13640.
45. Chevion, M. A Site-Specific Mechanism for Free Radical Induced Biological Damage: The Essential Role of Redox-Active Transition Metals. *Free Radical Biol. Med.* **1988**, *5*, 27–37.
46. Narayanan, R.; El-Sayed, M. A. Changing Catalytic Activity during Colloidal Platinum Nanocatalysis Due to Shape Changes: Electron-Transfer Reaction. *J. Am. Chem. Soc.* **2004**, *126*, 7194–7195.
47. Turkevich, J.; Stevenson, P. C.; Hillier, J. A Study of the Nucleation and Growth Processes in the Synthesis of Colloidal Gold. *Discuss. Faraday Soc.* **1951**, *11*, 55–75.
48. Besaratinia, A.; Synold, T. W.; Chen, H.-H.; Chang, C.; Xi, B.; Riggs, A. D.; Pfeifer, G. P. DNA Lesions Induced by UV A1 and B Radiation in Human Cells: Comparative Analyses in the Overall Genome and in the p53 Tumor Suppressor Gene. *Proc. Natl. Acad. Sci. U. S. A.* **2005**, *102*, 10058–10063.
49. Wei, H.; Cai, Q.; Rahn, R. O. Inhibition of UV Light- and Fenton Reaction-Induced Oxidative DNA Damage by the Soybcan Isoflavone Genistein. *Carcinogenesis* **1996**, *17*, 73–77.